Fluvial Dynamics Changes Driven by Illegal Gold Mining: A Land Use/Land Cover Analysis in the Ecuadorian Amazon

Isabel Adriana Chuizaca-Espinoza[1,2], Daniela Romero-Bermeo[1,3], Luciana das Dores de Jesus da Silva[4], Andrés Velastegui-Montoya[1,5]

[1] Laboratory of Geoinformation and Remote Sensing, ESPOL Polytechnic University, ESPOL, Campus Gustavo Galindo, Km. 30.5 Vía Perimetral, Guayaquil, 090902, Ecuador
[2] Postgraduate Program in Remote Sensing (PGSER). Coordination of Teaching, Research and Extension (COEPE). National Institute for Space Research (INPE). São José dos Campos, 12227-01 SP, Brazil
[3] Faculty of Life Sciences, ESPOL Polytechnic University, ESPOL, Campus Gustavo Galindo, Km. 30.5 Vía Perimetral, Guayaquil, 090902, Ecuador
[4] Department of Aquatic Systems, University of Concepción, Concepción 4070409, Chile
[5] Faculty of Engineering in Earth Sciences, ESPOL Polytechnic University, ESPOL, Campus Gustavo Galindo, Km. 30.5 Vía Perimetral, Guayaquil, 090902, Ecuador

Keywords: Ecuadorian Amazon, Nangaritza River, Land Use and Land Cover Changes, Illegal Mining, Fluvial Dynamics.

Abstract

Illegal alluvial mining has expanded rapidly across the Amazon basin, increasing pressure on river ecosystems, although its effects on fluvial dynamics during extreme hydrometeorological events remain insufficiently understood. This study examined land use and land cover (LULC) changes after a flooding and overflow event in the Nangaritza River and evaluated their influence on river dynamics. The objective was to determine the impacts of illegal mining on the fluvial behavior of the Nangaritza River in the southern Ecuadorian Amazon. Sentinel-2 Level-2A multispectral imagery was processed in Google Earth Engine to generate cloud-free mosaics for pre- and post-event conditions. Spectral indices including NDVI, MNDWI, NDTI, NDMI, and NDBaI improved classification accuracy. LULC maps were produced using the Random Forest supervised classification algorithm. Accuracy was evaluated with confusion matrices, while transition matrices and Map Algebra in ArcGIS Pro quantified spatial changes. Fluvial dynamics were assessed through variations in water bodies, mining areas, and sandbanks. Results showed a marked expansion of illegal mining along the river corridor through the conversion of forested, sedimentary, and aquatic surfaces into mining zones. These changes were accompanied by deforestation and transitions among clear water, turbid water, and sandbanks, indicating active sediment redistribution. Exchanges between water bodies and exposed sediments reflected shifts in erosion and deposition processes. Overall, illegal mining combined with extreme rainfall altered river morphology, sediment dynamics, and riparian land cover in the Amazonian fluvial system. The findings highlight growing environmental risks for biodiversity, water quality, and long-term stability of riparian ecosystems.

1. Introduction

The Amazon is the most biodiverse region on the planet and plays a key role in global climate regulation due to its capacity for CO_2 sequestration, its precipitation cycles, and its storage of approximately 20% of the world's freshwater resources (Coe et al., 2016; Sampaio et al., 2021; Schmitz et al., 2025). However, it is increasingly threatened by the expansion of anthropogenic activities such as mineral extraction (Mataveli et al., 2022), urban expansion (Santos et al., 2022), deforestation (da Silva et al., 2023), and forest fires (Lapola et al., 2023), all of which alter Amazonian ecosystems that host nearly 10% of global biodiversity. The intensification of these anthropogenic activities disrupts both terrestrial and aquatic ecosystems, exacerbating global warming and weakening the role of tropical forests as natural mitigators of climate change (Flores et al., 2024). Furthermore, these activities increase risks to human health due to heavy metal contamination in Amazonian rivers derived from extractive activities (Chuizaca-Espinoza et al., 2025c).

The Amazon region contains approximately 40% of the world's mineral reserves, contributing nearly 4% to the gross domestic product of Latin America (Doussoulin and Mougenot, 2022). The rapid increase in gold prices, road expansion, and limited economic opportunities have driven the growth of alluvial mining, both legal and illegal, even in remote areas of the Amazon (Larrea-Gallegos et al., 2023). Consequently, countries such as Brazil have experienced losses of ecosystem services, the emergence of neurodegenerative diseases, reductions in children's IQ, increased cancer incidence, and hydromorphological alterations of river systems (Gasparinnetti et al., 2024). Alluvial mining is primarily conducted along riverbeds and banks, where sediments are extracted to access economically valuable minerals, as evidenced in case studies from the Peruvian Amazon where illegal activities generate mercury and heavy metal contamination (Becerra-Lira et al., 2024).

Seasonal variations influence ecological and biogeochemical processes in rivers and their riparian zones, as well as the human and ecological activities occurring within them (Arora and Kumar, 2025). The presence of mining activities in a river can intensify flow dynamics and bedload transport, leading to modifications in the hydromorphodynamics of fluvial ecosystems (Dethier et al., 2023). Artisanal and small-scale mining in floodplains produces direct negative effects on fluvial habitats (Rentier and Cammeraat, 2022). Among the most significant impacts are alterations in the stability and composition of streambeds, changes in channel morphology, increased turbidity, variations in water velocity and depth, and changes in the quantity of woody debris within the channel (Bayazidy et al., 2024).

https://doi.org/10.5194/isprs-archives-XLIX-B3-2026-573-2026

In Ecuador, artisanal and small-scale mining (ASM) has become an important contributor to economic growth and national development (Mestanza-Ramón et al., 2022). However, by 2021, mining activities concentrated in the Ecuadorian Amazon covered approximately 7,495 hectares, generating significant impacts on water resources (Monitoring of the Amazon Program (MAAP), 2024). Among the most notable effects are alterations in river gradients, which intensify erosion processes, modify flow patterns, and compromise the stability of fluvial systems (Nguyen et al., 2025). Consequently, in the province of Zamora Chinchipe, the overflow of three rivers has been recorded, affecting approximately 500 families and causing economic losses exceeding USD 2 million in production.

The expansion of these activities within the Amazon biome highlights the importance of monitoring through remote sensing and Geographic Information Systems (GIS) to evaluate impacts and support decision-making (Santos et al., 2019). Previous studies have shown how territorial and ecological changes identified through land use and land cover (LULC) analysis affect the environment and generate social tensions by impacting the traditional livelihoods of Indigenous communities (Heredia-R et al., 2021). Additionally, these tools can serve as early warning systems to mitigate illegal activities by identifying mining hotspots in near real time (Chuizaca-Espinoza et al., 2025a). Furthermore, geospatial tools strengthen environmental decision-making processes, including the regulation of artisanal and small-scale mining within the Amazon region using open-access data (Rorato et al., 2020). Nevertheless, despite the vulnerability of Amazonian ecosystems to the impacts of ASM, the specific ways in which these mining activities influence riparian processes in the Ecuadorian Amazon remain insufficiently understood.

Remote sensing monitoring of mining expansion in the Amazon biome has become a tool for assessing the socio-environmental impacts of this extractive industry. In Ecuador, various studies analyze mining expansion through analyses of changes in land use and land cover, the effects of water turbidity, and physical-chemical laboratory tests of water and sediment samples (Patiño-Miñan et al., 2025; Romero-Bermeo et al., 2025; Velastegui-Montoya et al., 2024a). In the context of growing concern over the rapid expansion of illegal alluvial mining in the southern Ecuadorian Amazon, some questions remain unanswered: 1) How does land use and land cover (LULC) mapping contribute to the assessment of river dynamics? 2) What are the main LULC changes associated with the expansion of illegal mining? 3) What are the impacts of flooding and overflow events on the river dynamics of the Nangaritza River? This article aims to identify LULC changes along the banks of the Nangaritza River by processing Sentinel-2 satellite imagery and applying machine learning, to assess the effects of illegal mining on its river dynamics. The results can be used to propose mitigation, remediation, and environmental management strategies, thereby reducing the negative impacts of mining and safeguarding both ecosystems and local communities.

2. Study Area

The Nangaritza River is in southeastern Ecuador within the Amazon biome (Fig. 1a) and flows through the province of Zamora Chinchipe in a north–south direction (Fig. 1b). The study area corresponds to a 5 km buffer surrounding the Nangaritza River, defining the Area of Interest (AOI) with a total surface area of 1,286.03 km² (Fig. 1c). This region presents high socio-environmental complexity due to the spatial overlap of Indigenous territories, protected areas, and protective forests, notably including Podocarpus National Park and the Cerro Plateado Biological Reserve (Fig. 1c) (Ministerio del Ambiente, 2026). Within the AOI, 24 Indigenous territories were identified, both officially titled and non-recognized, primarily belonging to the Shuar and Saraguro peoples (RAISG, 2026), who directly depend on the Nangaritza River's fluvial system. The selection of the AOI responds to the high socio-environmental vulnerability of the Nangaritza River, as it represents one of the fluvial systems most affected by the expansion of illegal mining in the southern Ecuadorian Amazon, as well as by flooding and overflow events recorded in the province of Zamora Chinchipe during 2025 (Secretaría Nacional de Gestión de Riesgos (SNGRE), 2025). These conditions make the AOI a priority area for analyzing land use and land cover (LULC) changes and environmental risks associated with fluvial dynamics and illegal mining activities that impact riparian ecosystems and the communities settled in their immediate surroundings.

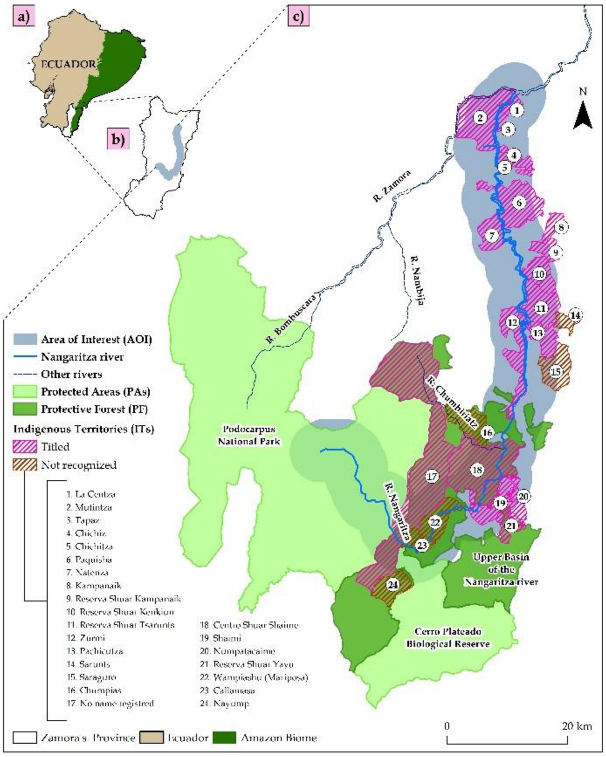

Figure 1. Study area Map. (a) Location of the province of Zamora Chinchipe within the Ecuadorian Amazon. (b) Location of the Area of Interest (AOI) in the province of Zamora Chinchipe. (c) Nangaritza river, other nearby rivers, Protected Areas (PAs), Protective Forest (PF) and Indigenous Territories (ITs).

3. Methodology

3.1 Data Acquisition and Preparation

The AOI polygon was imported into the Google Earth Engine (GEE) interface and projected to UTM Zone 18 South under the World Geodetic System 1984 (WGS 84) within the Universal Transverse Mercator (UTM) coordinate system to explore the available satellite imagery collections on the platform. Satellite images from the Harmonized Sentinel-2 MSI: Multispectral Instrument, Level-2A Image Collection were filtered according to data availability during the periods of interest within the AOI (European Union/ESA/Copernicus, 2025). The study periods correspond to the scenario prior to the flooding and overflow event in the Nangaritza River (July 2024 – March 2025) and the scenario following this event (April 2025 – December 2025) (Secretaría Nacional de Gestión de Riesgos (SNGRE), 2025). A total of 20 images with cloud cover below 30% were used for each period. A cloud and cloud-shadow masking function (MaskClouds for Sentinel-2) was applied (Chuizaca-Espinoza et al., 2025b), and a median reducer was used to generate cloud-free mosaics for each period.

3.2 Data Processing

The following spectral bands were considered: blue, green, red, water vapor, shortwave infrared 1, and near-infrared 1 and 2. Additionally, five spectral indices were calculated to improve land use and land cover (LULC) classification: i) the Normalized Difference Vegetation Index (NDVI) (Rouse et al., 1973), which allowed the distinction between forested areas and grasslands; ii) the Modified Normalized Difference Water Index (MNDWI) (Rouse et al., 1973), used to identify water bodies, meanders, and sinuous and braided channel sections; iii) the Normalized Difference Turbidity Index (NDTI) (Bid and Siddique, 2019), which separated water bodies according to the presence of suspended material; iv) the Normalized Difference Moisture Index (NDMI) (Velastegui-Montoya et al., 2024a), which helped identify sandbanks and mining lands; and v) the Normalized Difference Built-up Index (NDBaI) (Velastegui-Montoya et al., 2024c), used to delineate urban areas within the AOI. These indices were added as new bands to each composite to improve the performance of the classification model (Chuizaca-Espinoza et al., 2025b).

3.3 LULC Classification

The LULC classification was performed using the Random Forest (RF) algorithm. RF is a supervised machine learning classification algorithm widely used for detecting LULC changes on the Google Earth Engine platform (Pande et al., 2024). The RF algorithm generates multiple decision trees using a sample that is divided into subsets according to the most significant input variable (Velastegui-Montoya et al., 2024d). It then tries to create homogeneous sub nodes in relation to the target variable. The final RF output is determined by the class receiving the highest number of votes from the individual trees. The number of trees (parameter *ntree* within GEE) grown iteratively in the RF model to reach 100. If there are M input variables, a number $m < M$ is specified, resulting in m variables randomly selected from M (parameter *mtry* within GEE) for each node. The riverbanks of the Nangaritza River within the AOI were classified into seven LULC categories: Forest, Grasslands, Clear water, Turbid water, Mining lands, Sand banks, and Urban area. These categories were selected because they represent the main land cover types and land uses in the study area, as well as the environmental consequences associated with the reported flooding and overflow events (SNGRE, 2025). The selected LULC classes are described in Table 1.

Training samples for the pre-event scenario included 68,858 pixels for "Forest," 2,378 for "Grasslands," 40 for "Clear water," 1,396 for "Turbid water," 2,580 for "Mining lands," 697 for "Sand banks," and 1,168 for "Urban area." For the post-event scenario, the training samples consisted of 56,294 pixels for "Forest," 2,198 for "Grasslands," 83 for "Clear water," 1,319 for "Turbid water," 3,552 for "Mining lands," 560 for "Sand banks," and 1,872 for "Urban area" as training inputs for the RF model. A total of 100 iterations were performed. Subsequently, a random subset comprising 70% of the samples without replacement was selected to train the RF classifier. The remaining 30% of the dataset was used for validation to provide an independent evaluation of the model. To assess the accuracy of the LULC classification, a confusion matrix was generated for each scenario. The rows represent the LULC classes in the post-classified composition, while each column represents the reference LULC classes. The degree to which the results approach the values considered accurate is referred to as accuracy (Pal, 2005). Therefore, from the confusion matrix, consumer accuracy (CA), producer accuracy (PA), and overall accuracy (OA) were calculated (Junaid et al., 2023).

Classes	Descriptions
Forest	Non disturbed forest, dense forest and scrub
Grasslands	Low-density vegetation cover, mainly agricultural plots
Clear water	High transparency water and low presence of suspended sediments
Turbid water	Low transparency water and high presence of suspended sediments
Mining lands	Area of soil exposed by mineral extraction
Sand banks	Fluvial sandbanks and other types of sand deposits, including both wet and dry types
Urban area	Human constructions such as buildings and roads

Table 1. LULC classes selected and their descriptions.

3.4 Estimation of spatio-temporal LULC changes

To quantify and analyze changes, a comparison was conducted between the LULC classification results from the pre-event and post-event flooding and overflow scenarios by calculating two transition matrices. The LULC classification outputs from both scenarios were exported in GeoTIFF format from Google Earth Engine to ArcGIS Pro, where pixel-based area calculations were performed using a spatial resolution of 10 m. To identify changes such as persistence, gains, and losses in surface area, a transition matrix between classes was calculated by applying operations with the Map Algebra Calculator tool (Velastegui-Montoya et al., 2024b). Stable or unchanged areas were located along the main diagonal of the matrix. The remaining matrix positions represent values corresponding to transitions from one class to another between the initial and final dates. Row and column totals were summed to obtain the total area of each class and scenario. To determine whether a decrease occurred in a class, the persistence value was subtracted from the total class area at the beginning of the period. Likewise, persistence was subtracted from the final total area to estimate gains in each class.

3.5 Fluvial Dynamics identification

Finally, the raster of changes obtained during the transition matrix calculation process was used to identify the areas where classes associated with the active channel of the Nangaritza River (Clear water, Turbid water, Mining lands, and Sand banks) occurred in each scenario. This allowed the delimitation and quantification of the surfaces where the river migrated, deposited sediments, altered its turbidity, and reactivated adjacent channels. This step made it possible to better understand changes in fluvial dynamics and associate them with the event of interest. It also enabled the identification of the influence of illegal mining expansion on the Nangaritza River during the previously reported flooding and overflow event (SNGRE, 2025).

4. Results and Discussion

4.1 Accuracy Assessment

The accuracy assessment of the LULC classifications developed using the Random Forest algorithm was performed through confusion matrices constructed from independent validation samples. The matrices presented in Figure 2 allowed the comparison between predicted classes and reference classes, quantifying the performance of the RF model in terms of correct assignments and classification errors among the seven classes. Based on these matrices, the distribution of accuracy along the main diagonal and the patterns of confusion between classes were analyzed, providing a quantitative basis for interpreting the results for the two scenarios: before (Figure 2a) and after (Figure 2b) the flooding and overflow event along the Nangaritza River.

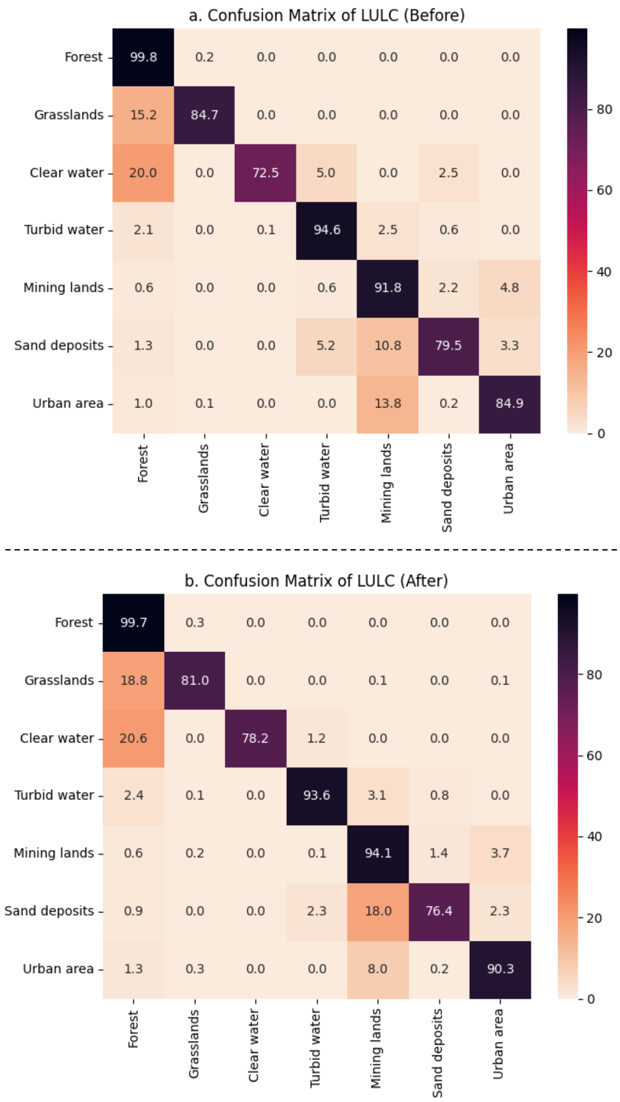

Figure 2. Confusion matrices for land use and land cover (LULC) classification obtained using the Random Forest algorithm. a) Pre-flood event scenario along the Nangaritza River (before). b) Post-flood event scenario (after). The values represent the percentage of misclassification between reference classes (rows) and predicted classes (columns).

In the scenario prior to the flooding and overflow event of July 2025 near the Nangaritza River, the confusion matrix shows a high overall performance of the LULC classification generated using the Random Forest algorithm, employing as predictive variables all bands from the cloud-free Sentinel-2 mosaic and the spectral indices NDVI, MNDWI, NDTI, NDMI, and NDBaI. The Forest class achieved the highest accuracy (99.8%), indicating a clear differentiation from other land cover types, largely supported by the NDVI. Similarly, Turbid water (94.6%) and Mining lands (91.8%) presented high accuracy levels, associated with the algorithm’s ability to capture variability in sediment load (NDTI) and soil moisture (NDMI). However, some confusion between classes was also identified. Grasslands were frequently misclassified as Forest (15.2%). Clear water showed classification errors toward Forest (20.0%) and Turbid water (5.0%), reflecting the complexity of mapping classes associated with fluvial dynamics prior to the event. In addition, Sand banks exhibited confusion with Mining lands (10.8%) and Turbid water (5.2%), while Urban area showed errors toward Mining lands (13.8%), possibly related to spectral similarities partially captured by the NDBaI and NDMI indices.

In the post-event scenario, the confusion matrix reveals changes in the performance of the LULC classification, reflecting modifications in the fluvial dynamics of the study area. An improvement is observed in the accuracy of Clear water (78.2%), attributed to better delineation of water bodies using the MNDWI index, as well as in Mining lands (94.1%) and Urban area (90.3%), indicating an enhanced ability of the model to differentiate exposed surfaces after the event. The Forest class maintained very high accuracy (99.7%), while Turbid water also retained high values (93.6%), although with a slight increase in confusion toward Mining lands (3.1%), which may be related to increased suspended sediments in the Nangaritza River following the flooding. Grasslands showed reduced accuracy (81.0%), with greater confusion toward Forest (18.8%), and Sand banks exhibited a notable increase in confusion with Mining lands (18.0%), suggesting the expansion or redistribution of alluvial materials and disturbed surfaces. Overall, these results indicate that the hydrological event influenced both landscape configuration and the spectral response of land cover types, affecting the model’s ability to discriminate between classes with similar characteristics and spectral signatures.

From the confusion matrix, consumer accuracy (CA), producer accuracy (PA), and overall accuracy (OA) were calculated. For the LULC classification prior to the flooding and overflowing event along the Nangaritza River, the overall accuracy was 0.96. The values obtained for consumer accuracy and producer accuracy for each class were as follows: 1) Forest (CA: 0.99, PA: 0.99), 2) Grasslands (CA: 0.95, PA: 0.84), 3) Clear water (CA: 0.93, PA: 0.63), 4) Turbid water (CA: 0.95, PA: 0.95), 5) Mining lands (CA: 0.83, PA: 0.92), 6) Sand banks (CA: 0.83, PA: 0.70), and 7) Urban area (CA: 0.86, PA: 0.85). For the LULC classification after the study event, the overall accuracy was 0.95. The consumer accuracy and producer accuracy values for each class were: 1) Forest (CA: 0.99, PA: 0.99), 2) Grasslands (CA: 0.89, PA: 0.76), 3) Clear water (CA: 1.00, PA: 0.68), 4) Turbid water (CA: 0.97, PA: 0.94), 5) Mining lands (CA: 0.89, PA: 0.93), 6) Sand banks (CA: 0.81, PA: 0.76), and 7) Urban area (CA: 0.92, PA: 0.90).

The comparison between consumer accuracy (CA) and producer accuracy (PA) reveals different patterns of omission and commission errors among classes in both scenarios. In the pre-event classification, the Forest class shows balanced values (CA and PA ≈ 0.99), indicating stability in both the identification of classified pixels and the representation of the reference class. In contrast, Grasslands and Clear water show differences between CA and PA (0.95 vs. 0.84 and 0.93 vs. 0.63, respectively), indicating omissions in the identification of these classes, particularly for Clear water. Mining lands presents a lower CA than PA (0.83 vs. 0.92), suggesting assignments from other classes into this category. In the post-event scenario, Forest maintains consistent values, while Clear water reaches a CA of 1.00 and a PA of 0.68, indicating that pixels classified as this class correspond entirely to the reference, although not all existing cases are captured. Grasslands shows a reduction in both indicators (CA: 0.89, PA: 0.76), while Sand banks maintains differences between CA and PA, reflecting persistent confusion with other land cover types. Overall, variations between CA and PA across both scenarios highlight changes in omission and commission patterns associated with landscape modifications and shifts in land cover distribution following the hydrological event.

4.2 LULC Net Changes

Net changes in land use and land cover classes reveal a reconfiguration of the landscape along the margins of the Nangaritza River following the flooding and overflow event (Figure 3). The Forest class showed a decrease of 3,830.38 ha, indicating a reduction in forest cover that may be linked to both flood-induced removal and deforestation. In contrast, the Grasslands class recorded an increase of 2,893.27 ha, suggesting a transition from previously forested areas to open land cover, possibly associated with disturbances during the period or with vegetation regeneration processes. Likewise, the Mining Lands class increased by 691.81 ha, evidencing the expansion of illegal mining, which may be associated with the conversion of previously forested areas, in addition to affecting soil conditions and local hydrology in Nangaritza. Classes related to water dynamics, such as Clear Water and Turbid Water, showed increases of 174.92 and 235.92 ha, respectively, indicating changes in water distribution and sediment load consistent with processes of flooding, erosion, and river transport. Meanwhile, Sand banks showed a reduction of 31.19 ha, which could be associated with the redistribution of sediments within the river system. Meanwhile, Urban Area showed a decrease of 134.35 ha, which may be related to direct impacts of the flooding and overflow events on the neighboring villages. Together, these changes reflect the interaction between fluvial processes intensified by the flood event and human activities in the reorganization of the landscape.

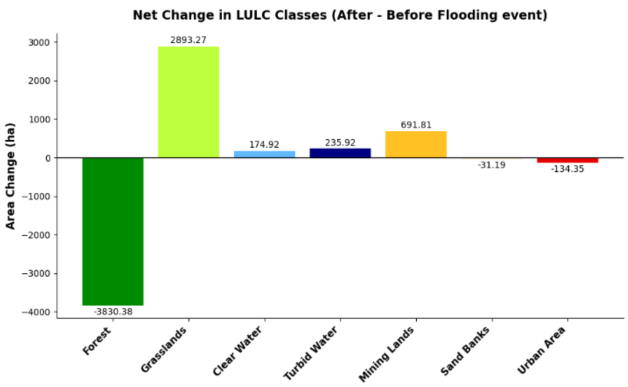

Figure 3. Net changes (After–Before) in land use and land cover (LULC) classes along the banks of the Nangaritza River. Positive values indicate gains and negative values indicate losses in area (ha) following the flooding and overflow event.

4.3 LULC Classes Transitions

To understand the processes underlying observed net changes, changes between land use and land cover classes were calculated using a transition matrix (Figure 4). In this matrix, the main diagonal groups the persistence of each class between the two periods analyzed. Meanwhile, the cells outside the diagonal correspond to the specific changes between classes. In this way, it was possible to identify not only which classes remained, but also what changes occurred between them following the flooding and overflowing of the Nangaritza River.

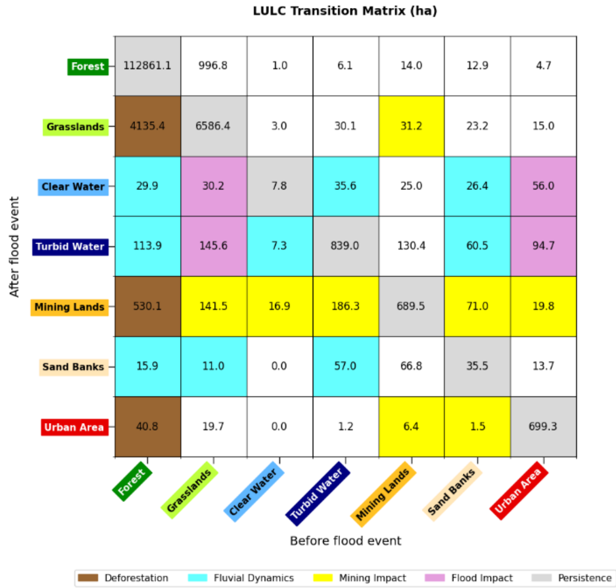

Figure 4. Transition matrix between the two sceneries of analysis. The main diagonal represents the persistence areas during the periods. Deforestation, Fluvial Dynamics, Mining Impact and Flood Impact areas associated were identified.

The main diagonal of the matrix shows persistence across several classes, particularly in Forest (112,861.1 ha), Grasslands (6,586.4 ha), and Mining Lands (689.5 ha), indicating that part of this coverage remains unchanged between the two periods analyzed. This pattern reflects that, despite the observed changes, there are areas that retain their initial condition, especially in forested areas and in areas previously affected by mining activities. Transitions associated with deforestation indicate the conversion of Forest areas into other land cover types, primarily Grasslands (4,135.4 ha) and Mining lands (530.1 ha), and to a lesser extent into Urban area (40.8 ha). Additionally, a transition from Grasslands to Forest (996.8 ha) was observed, suggesting dynamics of change and possible vegetation regeneration following increased rainfall. Together, these transitions indicate a loss of forested cover associated with conversion to open land types and areas altered by human activities.

Transitions associated with river dynamics reveal interactions between land cover, water bodies, and sediment surfaces. Conversions are observed from Forest to Clear Water (29.9 ha), Turbid Water (113.9 ha), and Sand Banks (15.9 ha), as well as from Grasslands to Sand Banks (11.0 ha), indicating the incorporation of previously vegetated areas into the river system. Among the water classes, bidirectional exchanges are identified between Clear Water and Turbid Water (7.3 ha and 35.6 ha, respectively), reflecting variations in sediment load. Likewise, transitions from Sand Banks to Clear Water (26.4 ha) and Turbid Water (60.5 ha) are recorded, along with conversions from Turbid Water to Sand Banks (57.0 ha), which demonstrates the alternation between flooded and exposed areas in the Nangaritza River. Taken together, these transitions reveal an active dynamic of water and sediment redistribution within the river system.

For the impact of mining on LULC along the riverside of the Nangaritza river, it was found that: 141.5 ha of Grasslands, 16.9 ha of Clear water, 186.3 ha of Turbid water, and 71 ha of Sand banks were converted to Mining lands. These changes are associated with the type of mining practiced in the AOI, which is illegal alluvial gold mining; following a flood and overflow event, this directly impacts the land cover classes associated with the riverine context. The transitions identified as flood impacts show changes between water classes and anthropogenic zones, notably the shifts from Grassland to Clear water (30.2 ha) and to Turbid water (145.6 ha). Also, from Urban Area to Clear water (56 ha) and to Turbid water (94.7 ha). These conversions suggest the temporary expansion of water over anthropogenic surfaces and developed areas, consistent with the impacts reported in villages and livestock-raising areas following the flooding and overflow event on the Nangaritza River.

4.4 Spatio-Temporal LULC changes and Mining Impact Assessment

To spatially assess changes in the riversides of the Nangaritza River resulting from flooding and overflow events, a thematic map was created to illustrate LULC changes (Figure 5). Four Mining Impact Interest Zones (MIIZ) were identified, representing the scattered mining activity sites along the main river channel. This multitemporal comparison and the focused analysis of the MIIZs are presented below.

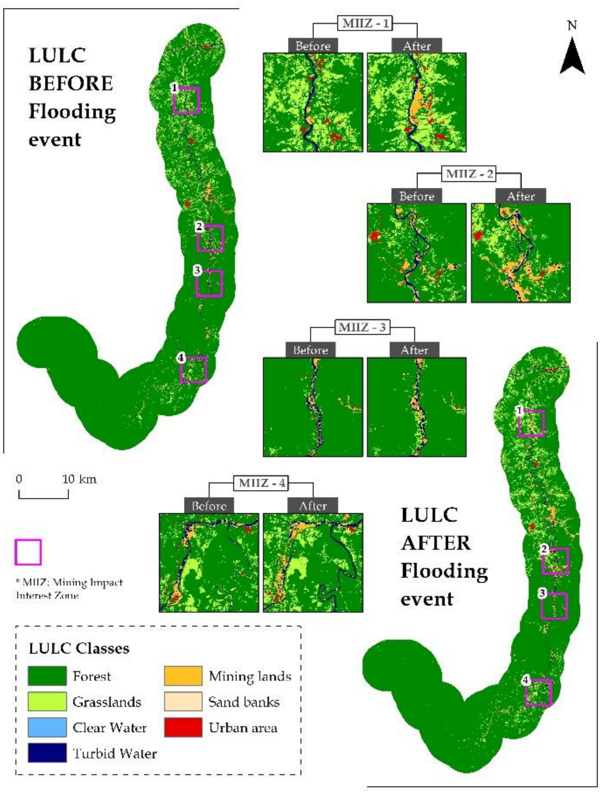

Figure 5. Thematic map of LULC sceneries (Before and After Flooding event). MIIZ – 1 to MIIZ – 4 represents the main areas of illegal mining expansion in the Nangaritza river.

The forest category decreased after the flood, resulting in a total loss of 3,830.38 hectares. Most of this reduction was due to conversions into grasslands and mining lands. A notable transition toward turbid water was also observed. This pattern indicates both deforestation and alterations in river dynamics. In the maps, these changes are particularly evident in the MIIZ zones (I and IV), where sediment-laden water increased after the river overflowed. This suggests that the flood not only mobilized materials and eroded riverbanks but also created openings that facilitated mining activities in areas previously covered by forest, contributing to greater landscape fragmentation.

After the flood, grasslands expanded by a total of 2,893.27 hectares. The data indicate that most of this increase occurred in areas previously occupied by forest, with a loss of 4,135.42 hectares. This suggests forest degradation following the flood event. However, grasslands also remained stable across a large portion of their surface, with 6,586.43 hectares unchanged. This stability indicates that grasslands may be relatively resilient in areas less affected by mining activities. In some zones, satellite imagery confirms the expansion of open surfaces and secondary vegetation. This expansion is likely related to the deposition of fine sediments and disturbances in water flow, which prevented immediate forest regeneration. Such changes are significant because they increase ecosystem vulnerability to mining and other human activities.

The turbid water class experienced one of the most notable changes, with a total increase of 235.92 hectares. This reflects the strong influence of the flood on river flow dynamics. Transition analysis shows significant changes from clear water, grasslands, and forest toward turbid water. This pattern is consistent with field observations and satellite imagery showing increased turbidity after the flood event. The increase is associated with intense erosion, sediment mobilization, and disturbances caused by both the flood and pre-existing mining activities. In two study areas (MIIZ II and III), the flood appears to have dispersed mining residues and fine sediments throughout the river system, amplifying their distribution.

Mining lands increased by 691.81 hectares, representing a substantial change within the MIIZ areas. Most of this increase originated from former grasslands (141.47 hectares) and forest areas (530.10 hectares), as well as 130.36 hectares previously classified as turbid water. These results indicate a rapid expansion of human activities following the flood. This pattern suggests that the flood facilitated access to and exploitation of new areas for mining. This trend is especially visible in MIIZ I and IV, where maps show an increase in yellow patches representing mining activities. The expansion of mining lands after the flood creates an additional concern, as mining not only takes advantage of post-flood landscape changes but may also increase the vulnerability of the river system to future flooding events.

5. Conclusions

The results indicate that the most significant LULC changes associated with the flooding and overflow event occurred in areas located along the Nangaritza River, particularly within the MIIZ zones I and IV. In these areas, the spatial analysis revealed a notable reduction in forest cover and the expansion of grasslands, mining lands, and turbid water surfaces. The loss of 3,830.38 hectares of forest demonstrates that the flood event, combined with existing anthropogenic pressures, significantly altered the landscape structure. These changes highlight that flood-related disturbances were spatially concentrated near the river corridor and in areas already influenced by mining activities.

The flood event also produced clear impacts on the fluvial dynamics of the Nangaritza River. The increase in turbid water of 235.92 hectares indicates intensified sediment transport and riverbank erosion following the overflow. Transitions from clear water, forest, and grasslands to turbid water reflect the mobilization of sediments and the redistribution of alluvial materials along the river channel. These patterns were particularly evident in MIIZ II and III, where the dispersion of fine sediments and mining residues suggests that the flood acted as a mechanism that amplified sediment loads and altered water quality. Consequently, the hydrological disturbance not only modified land cover patterns but also affected the physical and sedimentary dynamics of the river system.

The results also demonstrate that illegal or uncontrolled mining activities play an important role in shaping the fluvial dynamics of the Nangaritza River. The expansion of mining lands by 691.81 hectares, mainly replacing forest and grassland areas, indicates that mining intensified following the flood event. The spatial distribution of these new mining areas, especially in MIIZ I and IV, suggests that the flood facilitated access to previously forested areas and exposed surfaces suitable for extraction activities. At the same time, the interaction between mining and hydrological processes appears to increase sediment mobilization and water turbidity, reinforcing the disturbance of the river system. Overall, the study shows that the flooding and overflow event acted as a triggering factor that accelerated land cover transitions and intensified the interaction between natural hydrological processes and human activities. The combined effects of deforestation, sediment redistribution, and mining expansion contribute to increased landscape fragmentation and greater vulnerability of the Nangaritza River basin to future hydrological disturbances. These findings highlight the importance of strengthening environmental monitoring and territorial management strategies to mitigate the impacts of mining activities and protect the ecological stability of the river system.

Acknowledgements

This work was supported by Nacional Agency for Research and Development of Chilean Government ANID, FONDECYT Postdoctorado ANID Nº 3240641.

References

Arora, S., Kumar, B., 2025. Effects of proximity of the sediment mining pit on riverbank stability. Sci. Rep. 15, 10389. https://doi.org/10.1038/s41598-025-95524-7

Bayazidy, M., Maleki, M., Khosravi, A., Shadjou, A.M., Wang, J., Rustum, R., Morovati, R., 2024. Assessing Riverbank Change Caused by Sand Mining and Waste Disposal Using Web-Based Volunteered Geographic Information. Water (Basel). 16, 734. https://doi.org/10.3390/w16050734

Becerra-Lira, E., Rodriguez-Achata, L., Muñoz Ushñahua, A., Corvera Gomringer, R., Thomas, E., Garate-Quispe, J., Hilares Vargas, L., Nascimento Herbay, P.R., Gamarra Miranda, L.A., Umpiérrez, E., Guerrero Barrantes, J.A., Pillaca, M., Cusi Auca, E., Peña Valdeiglesias, J., Russo, R., del Castillo Torres, D., Velasquez Ramírez, M.G., 2024. Spatio-temporal trends of mercury levels in alluvial gold mining spoils areas monitored between rainy and dry seasons in the Peruvian Amazon. Environ. Res. 245, 118073. https://doi.org/10.1016/j.envres.2023.118073

Bid, S., Siddique, G., 2019. Identification of seasonal variation of water turbidity using NDTI method in Panchet Hill Dam, India. Model. Earth Syst. Environ. 5, 1179–1200. https://doi.org/10.1007/s40808-019-00609-8

Chuizaca-Espinoza, I.A., Adorno, B.V., Velastegui-Montoya, A., Amaral, S., 2025a. Illegal Mining in Amazonian Indigenous Lands: Analysis of Hotspots and impacted households, in: XXI Simpósio Brasileiro de Sensoriamento Remoto (SBSR) 2025. Salvador, Bahia.

Chuizaca-Espinoza, I.A., Mora-Mejía, S., Carvalho Guimarães, Y., Nogueira de Andrade, M.M., Meiguins de Lima, A.M., Amaral, S., Velastegui-Montoya, A., 2025b. Land Use Land Cover to assess the impact of Hydroelectric Project on River Dynamics in the Upper Amazon, in: Anais Do XXI Simpósio Brasileiro de Sensoriamento Remoto.

Chuizaca-Espinoza, I.A., Velastegui-Montoya, A.D., Amaral, S., 2025c. Mining-Driven Land Use and Land Cover Changes in Quilombola Territories of the Brazilian Amazon, in: 2nd International Electronic Conference on Land, Online.

Coe, M.T., Macedo, M.N., Brando, P.M., Lefebvre, P., Panday, P., Silvério, D., 2016. The Hydrology and Energy Balance of the Amazon Basin. pp. 35–53. https://doi.org/10.1007/978-3-662-49902-3_3

da Silva, C.F.A., de Andrade, M.O., dos Santos, A.M., de Melo, S.N., 2023. Road network and deforestation of indigenous lands in the Brazilian Amazon. Transp. Res. D Transp. Environ. 119, 103735. https://doi.org/10.1016/j.trd.2023.103735

Dethier, E.N., Silman, M., Leiva, J.D., Alqahtani, S., Fernandez, L.E., Pauca, P., Çamalan, S., Tomhave, P., Magilligan, F.J., Renshaw, C.E., Lutz, D.A., 2023. A global rise in alluvial mining increases sediment load in tropical rivers. Nature 620, 787–793. https://doi.org/10.1038/s41586-023-06309-9

Doussoulin, J.P., Mougenot, B., 2022. Mapping mining and ecological distribution conflicts in Latin America, a bibliometric analysis. Resources Policy 77, 102650. https://doi.org/10.1016/j.resourpol.2022.102650

European Union/ESA/Copernicus, 2025. Harmonized Sentinel-2 MSI: MultiSpectral Instrument, Level-2A [WWW Document]. Google Earth Engine. URL https://developers.google.com/earth-engine/datasets/catalog/COPERNICUS_S2_SR_HARMONIZED (accessed 10.27.24).

Flores, B.M., Montoya, E., Sakschewski, B., Nascimento, N., Staal, A., Betts, R.A., Levis, C., Lapola, D.M., Esquível-Muelbert, A., Jakovac, C., Nobre, C.A., Oliveira, R.S., Borma, L.S., Nian, D., Boers, N., Hecht, S.B., ter Steege, H., Arieira, J., Lucas, I.L., Berenguer, E., Marengo, J.A., Gatti, L. V., Mattos, C.R.C., Hirota, M., 2024. Critical transitions in the Amazon forest system. Nature 626, 555–564. https://doi.org/10.1038/s41586-023-06970-0

Gasparinnetti, P., Bakker, L.B., Queiroz, J.M., Vilela, T., 2024. Economic valuation of artisanal small-scale gold mining impacts: A framework for value transfer application. Resources Policy 88, 104259. https://doi.org/10.1016/j.resourpol.2023.104259

Heredia-R, M., Torres, B., Cabrera-Torres, F., Torres, E., Díaz-Ambrona, C.G.H., Pappalardo, S.E., 2021. Land Use and Land Cover Changes in the Diversity and Life Zone for Uncontacted Indigenous People: Deforestation Hotspots in the Yasuní Biosphere Reserve, Ecuadorian Amazon. Forests 12, 1539. https://doi.org/10.3390/f12111539

Junaid, M., Sun, J., Iqbal, A., Sohail, M., Zafar, S., Khan, A., 2023. Mapping LULC Dynamics and Its Potential Implication on Forest Cover in Malam Jabba Region with Landsat Time Series Imagery and Random Forest Classification. Sustainability 15, 1858. https://doi.org/10.3390/su15031858

Lapola, D.M., Pinho, P., Barlow, J., Aragão, L.E.O.C., Berenguer, E., Carmenta, R., Liddy, H.M., Seixas, H., Silva, C.V.J., Silva-Junior, C.H.L., Alencar, A.A.C., Anderson, L.O., Armenteras, D., Brovkin, V., Calders, K., Chambers, J., Chini, L., Costa, M.H., Faria, B.L., Fearnside, P.M., Ferreira, J., Gatti, L., Gutierrez-Velez, V.H., Han, Z., Hibbard, K., Koven, C., Lawrence, P., Pongratz, J., Portela, B.T.T., Rounsevell, M., Ruane, A.C., Schaldach, R., da Silva, S.S., von Randow, C., Walker, W.S., 2023. The drivers and impacts of Amazon forest degradation. Science (1979). 379. https://doi.org/10.1126/science.abp8622

Larrea-Gallegos, G., Kahhat, R., Vázquez-Rowe, I., Parodi, E., 2023. A machine learning approach to understand how accessibility influences alluvial gold mining expansion in the Peruvian Amazon. Case Studies in Chemical and Environmental Engineering 7, 100353. https://doi.org/10.1016/j.cscee.2023.100353

Mataveli, G., Chaves, M., Guerrero, J., Escobar-Silva, E.V., Conceição, K., de Oliveira, G., 2022. Mining Is a Growing Threat within Indigenous Lands of the Brazilian Amazon. Remote Sens. (Basel). 14, 4092. https://doi.org/10.3390/rs14164092

Mestanza-Ramón, C., Cuenca-Cumbicus, J., D’Orio, G., Flores-Toala, J., Segovia-Cáceres, S., Bonilla-Bonilla, A., Straface, S., 2022. Gold Mining in the Amazon Region of Ecuador: History and a Review of Its Socio-Environmental Impacts. Land (Basel). 11, 221. https://doi.org/10.3390/land11020221

Ministerio del Ambiente, A. y T.E. (MAATE), 2026. Mapa Interactivo. Geoportal. URL: https://ide.ambiente.gob.ec/mapainteractivo/

Monitoring of the Amazon Program (MAAP), 2024. Biblioteca Digital: Informes Destacados. URL: https://www.maapprogram.org/es/biblioteca-digital/

Nguyen, B.Q., Kantoush, S.A., Sumi, T., 2025. Assessing the multidimensional impacts of riverbed sand mining on geomorphological change and water transfer rate: A comprehensive investigation of Central Vietnam’s Vu Gia Thu Bon River system. J. Hydrol. (Amst). 654, 132853. https://doi.org/10.1016/j.jhydrol.2025.132853

Pal, M., 2005. Random forest classifier for remote sensing classification. Int. J. Remote Sens. 26, 217–222. https://doi.org/10.1080/01431160412331269698

Pande, C.B., Srivastava, A., Moharir, K.N., Radwan, N., Mohd Sidek, L., Alshehri, F., Pal, S.C., Tolche, A.D., Zhran, M., 2024. Characterizing land use/land cover change dynamics by an enhanced random forest machine learning model: a Google Earth Engine implementation. Environ. Sci. Eur. 36, 84. https://doi.org/10.1186/s12302-024-00901-0

Patiño-Miñan, A., Chuizaca-Espinoza, I.A., Miguel, V.R.S., Maia, A.B., Bulatov, D., Helmholz, P., Raiol, L.L., Velastegui-Montoya, A., 2025. Assessing Mining Pressure in the Ecuadorian Amazon: Analysis of environmental and social impacts, in: IGARSS 2025 - 2025 IEEE International Geoscience and Remote Sensing Symposium. pp. 3310–3315. https://doi.org/10.1109/IGARSS55030.2025.11243422

Red Amazónica de Información Socioambiental Georreferenciada (RAISG), 2026. Mapa en línea: Información geoespacial sobre la Amazonía. Datos cartográficos: Visualización de información geoespacial sobre la Amazonía. URL: https://www3.socioambiental.org/geo/RAISGMapaOnline/

Rentier, E.S., Cammeraat, L.H., 2022. The environmental impacts of river sand mining. Science of The Total Environment 838, 155877. https://doi.org/10.1016/j.scitotenv.2022.155877

Romero-Bermeo, D., Chuizaca-Espinoza, I.A., Brito Maia, A., San Miguel, V.R., Bulatov, D., Helmholz, P., Boumahdi, M., Molano Cárdenas, S.M., Carolina Rodrigues Santos, D., Raiol, L.L., Velastegui-Montoya, A., 2025. Mining in the Southern Ecuadorian Amazon: Hotspots analysis and regulatory efficiency, in: IGARSS 2025 - 2025 IEEE International Geoscience and Remote Sensing Symposium. pp. 3182–3186. https://doi.org/10.1109/IGARSS55030.2025.11243279

Rorato, A.C., Camara, G., Escada, M.I.S., Picoli, M.C.A., Moreira, T., Verstegen, J.A., 2020. Brazilian amazon indigenous peoples threatened by mining bill. Environmental Research Letters 15, 1040a3. https://doi.org/10.1088/1748-9326/abb428
Rouse, J.W., Haas, R.H., Schell, J.A., Deering, D.W., 1973.

Monitoring Vegetation Systems in the Great Plains with ERTS (Earth Resources Technology Satellite), in: Proceedings of 3rd Earth Resources Technology Satellite Symposium. Greenbelt, pp. 309–317.

Sampaio, G., Shimizu, M.H., Guimarães-Júnior, C.A., Alexandre, F., Guatura, M., Cardoso, M., Domingues, T.F., Rammig, A., von Randow, C., Rezende, L.F.C., Lapola, D.M., 2021. CO2 physiological effect can cause rainfall decrease as strong as large-scale deforestation in the Amazon. Biogeosciences 18, 2511–2525. https://doi.org/10.5194/bg-18-2511-2021

Santos, F., Graw, V., Bonilla, S., 2019. A geographically weighted random forest approach for evaluate forest change drivers in the Northern Ecuadorian Amazon. PLoS One 14, e0226224. https://doi.org/10.1371/journal.pone.0226224

Schmitz, M.H., Malek, Ž., do Couto, E.V., Gentil, E., Cardozo, A.L.P., Moretto, Y., da Silveira, N.S., Agostinho, A.A., 2025. Unsustainable land use trajectories in the Tocantins/Araguaia basin: Insights from future scenario modeling. Ambio 54, 1185–1198. https://doi.org/10.1007/s13280-025-02137-5

Secretaría Nacional de Gestión de Riesgos (SNGRE), 2025. SitRep No. 4 – Lluvias Zamora Chinchipe: INFORME DE SITUACIÓN PROVINCIAL. Zamora Chinchipe.

Velastegui-Montoya, A., Chuizaca-Espinoza, I.A., Alberto Falquez-Chávez, C., Aguilar-Aguilar, M., Bulatov, D., Carrión-Mero, P., 2024a. Assessment of Land Use/Land Cover Changes Due to Mining Activity in the Ecuadorian Amazon, in: IGARSS 2024 - 2024 IEEE International Geoscience and Remote Sensing Symposium. IEEE, pp. 5469–5473. https://doi.org/10.1109/IGARSS53475.2024.10642414

Velastegui-Montoya, A., García-Romero, J.A., Chuizaca-Espinoza, I.A., Quevedo, R.P., Santana-Cunha, C., Ochoa-Brito, J.I., Arias-Hidalgo, M., 2024b. Assessing regressive erosion effects: Unveiling riverside land use land cover changes post hydroelectric project construction. Environmental Challenges 15, 100882. https://doi.org/10.1016/j.envc.2024.100882

Velastegui-Montoya, A., Mora-Mejía, S., Chuizaca-Espinoza, I.A., Peña-Villacreses, G., Mishra, V., Ochoa-Brito, J.I., 2024c. Sustainable Development Challenges in the Ecuadorian Amazon: A Case Study of Land Use Affect and Landslide Risks Induced by a Hydropower Plant, in: IGARSS 2024 - 2024 IEEE International Geoscience and Remote Sensing Symposium. IEEE, pp. 4178–4182. https://doi.org/10.1109/IGARSS53475.2024.10642788

Velastegui-Montoya, A., Zhirzhan-Azanza, B., Rivera-Torres, H., Peña-Villacreses, G., Chuizaca-Espinoza, I.A., El Imanni, H.S., Brito, J.O., 2024d. Google Earth Engine for an Analyze of Land Use and Land Cover within an Oil Block in the Ecuadorian Amazon, in: IGARSS 2024 - 2024 IEEE International Geoscience and Remote Sensing Symposium. IEEE, pp. 4851–4855. https://doi.org/10.1109/IGARSS53475.2024.10641590